

Robust 3D gravity gradient inversion by planting anomalous densities

Leonardo Uieda* and Valéria C. F. Barbosa, *Observatório Nacional*

SUMMARY

We present a new gravity gradient inversion method for estimating a 3D density-contrast distribution defined on a grid of prisms. Our method consists of an iterative algorithm that does not require the solution of a large equation system. Instead, the solution grows systematically around user-specified prismatic elements called “seeds”. Each seed can be assigned a different density contrast, allowing the interpretation of multiple bodies with different density contrasts and that produce interfering gravitational effects. The compactness of the solution around the seeds is imposed by means of a regularizing function. The solution grows by the accretion of neighboring prisms of the current solution. The prisms for the accretion are chosen by systematically searching the set of current neighboring prisms. Therefore, this approach allows that the columns of the Jacobian matrix be calculated on demand, which greatly reduces the demand of computer memory and processing time. Tests on synthetic data and on real data collected over an iron ore province of Quadrilátero Ferrífero, southeastern Brazil, confirmed the ability of our method in detecting sharp and compact bodies.

INTRODUCTION

Over the past 20 years, substantial effort has been directed towards estimating 3D density-contrast distributions from gravity data inversion. Usually the inversion methods, like that of Li and Oldenburg (1998), produce blurred images of anomalous sources. On the other hand, methods for producing sharp images have been developed by Portniaguine and Zhdanov (2002) and Silva Dias et al. (2009). All previously mentioned methods require the solution of large linear systems, which can be one of the biggest hurdles for large problems. Attempts to overcome this problem include: the method of René (1986) that obtains 2D sharp and compact bodies by successively incorporating cells around pre-specified cells called “seeds” with known density contrasts; and the method of Camacho et al. (2000) that recovers sharp 3D bodies by means of a systematic search algorithm. We present a new 3D gravity inversion that uses “seeds” around which the density anomalies grow, as in René (1986), and imposes compactness of the solution using a regularizing function like that of Silva Dias et al. (2009). Tests on synthetic data and on field data collected over the Quadrilátero Ferrífero, southeastern Brazil, confirmed the potential of the method in producing sharp images of the density anomalies.

INVERSE PROBLEM

Consider a data set composed of N observations of components of the gravity gradient tensor. We assume that these observations are due to anomalous densities confined within a three-dimensional region of the subsurface. Let us consider that this region is divided into a set of M juxtaposed right

rectangular prisms. It follows that the gravity gradient tensor caused by the density anomalies can be approximated by the sum of the contribution of each prism, which can be calculated using the formulas of Nagy et al. (2000). Assuming that each prism has a constant density contrast, it follows that the relationship between the components of the gravity gradient tensor and the density contrast of each prism is linear and can be expressed in matrix notation as

$$\mathbf{d} = \mathbf{G}\mathbf{p}, \quad (1)$$

where \mathbf{d} is the data vector containing the gravity gradient tensor components caused by the prism ensemble, \mathbf{p} is the parameter vector containing the density contrast of each prism, and \mathbf{G} is the Jacobian matrix of the functional relation between \mathbf{d} and \mathbf{p} .

The inverse problem of estimating \mathbf{p} is an ill-posed problem and thus requires additional constraints to be solved. The constraints used in our method impose that the solution be compact and concentrated around “seeds”, which are user-specified prisms with known density contrasts. These conditions can be imposed by means of a regularizing function following the approach of Silva Dias et al. (2009). We formulate the inverse problem as minimizing the goal function

$$\Gamma(\mathbf{p}) = \phi(\mathbf{p}) + \mu\theta(\mathbf{p}), \quad (2)$$

where μ is a regularizing parameter. Function $\phi(\mathbf{p})$ is a measure of the data misfit and is usually the ℓ_2 norm of the residuals, which is sensitive to outliers in the data. If a more robust inversion is desired, the ℓ_1 norm of the residuals should be used

$$\phi(\mathbf{p}) = \|\mathbf{d}^o - \mathbf{d}\|_1 = \sum_{i=1}^N |d_i^o - d_i|, \quad (3)$$

where \mathbf{d}^o is a vector containing the measured data and \mathbf{d} is given by equation 1. It is important to note that we use the term “outliers” to refer to both errors in the measurements and to interfering gravitational effects produced by non-targeted sources.

The regularizing function $\theta(\mathbf{p})$ is similar to that of Silva Dias et al. (2009). It enforces the compactness of the solution around the seeds and is defined as

$$\theta(\mathbf{p}) = \sum_{i=1}^M \frac{p_i}{p_i + \varepsilon} l_i^\beta, \quad (4)$$

where p_i is the i th element of \mathbf{p} , ε is a small and positive constant used to avoid discontinuities, l_i is the distance between the i th prism and the seed to which it will be accreted, and β is the power to which l_i is raised and controls the compactness of the solution.

Planting algorithm

Our algorithm requires a set of N_S seeds specified by the user beforehand. These seeds should be chosen according to prior

Robust 3D gravity gradient inversion

information about the density anomalies, such as geologic models, well logs and previous inversions. Each seed consists of a prism of the interpretative model and thus the s th seed is described by a density-contrast value ρ_s and a position index i_s in the parameter vector. The algorithm starts with an initial estimate \mathbf{p}^0 with all elements set to zero. Next, the seeds are included in the initial estimate by setting $p_{i_s}^0 = \rho_s$. An iteration of the algorithm consists of trying to grow each of the N_S seeds by performing the accretion of one of its neighboring prisms. The accretion of a prism to the s th seed is performed in three steps:

1. Each neighboring prism of the seed is temporarily added to the estimate, one at a time, and the goal function (equation 2) is evaluated for the current estimate including the neighbor. Each neighbor is added to the estimate with the density contrast ρ_s of the s th seed.
2. One of the tested neighbors is chosen that both reduces the data-misfit function (equation 3) and provides the smallest value of the goal function (equation 2). This chosen neighbor is then added permanently to the estimate, finalizing the accretion. If none of the neighboring prisms of the s th seed meet these criteria then the s th seed doesn't grow in this iteration.
3. In the case that a neighboring prism is accreted to the s th seed, its neighboring prisms are appended to the seed's current neighbor list and the values of the goal and data-misfit functions are updated.

These three accretion steps are repeated for each seed. After all seeds have tried to grow a new iteration is started. This process stops when none of the seeds are able to grow, signifying that the data-misfit function (equation 3) cannot decrease further. Figure 1 shows a 2D sketch of three stages of the algorithm: the starting configuration; the end of the first iteration; and the final solution.

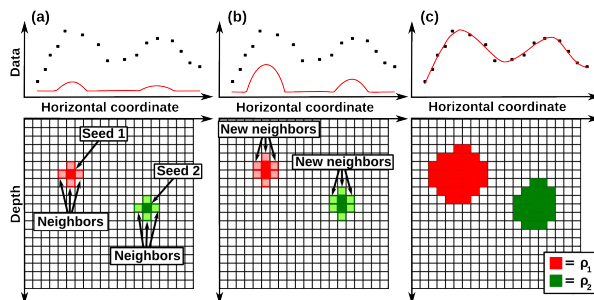


Figure 1: 2D sketch of three stages of the planting algorithm. **a)** Starting configuration using two seeds (dark red and dark green prisms). Neighbors are shown in light red and light green. **b)** State of the solution after the first iteration. **c)** The final result of the inversion after the algorithm stops.

One of the main advantages of our algorithm is that it does not require the solution of an equation system. Even more importantly, the full Jacobian matrix \mathbf{G} is not needed at any single time since the search is limited to neighboring prisms of the current solution. This means that each column of \mathbf{G}

only needs to be calculated when the prism of the interpretative model to which it refers becomes a neighbor of the current solution. This technique is known in computer science as “lazy evaluation”. Furthermore, once a neighboring prism is permanently added to the solution, its corresponding column is no longer needed and can be discarded. This results in fast inversion times and low memory usage, allowing the inversion of large data sets using fine meshes without the need for supercomputers or data compression algorithms (Portniaguine and Zhdanov, 2002). Another advantage is that there is no need to calculate the derivative of the goal function with respect to the parameters. Therefore, either the ℓ_2 , the ℓ_1 , or any order norm of the residuals, weighted or not, can be used without any modification to the algorithm.

APPLICATION TO SYNTHETIC DATA

Figure 2a-c shows the synthetic gravity gradient data used to test the performance and correctness of our method. The data set was produced by seven rectangular blocks with different geometries, depths and density contrasts (Figure 3a). The synthetic model was designed to simulate a real world scenario in which there are interfering gravitational effects produced by multiple sources, some of which are not of interest to the interpretation. In this case, we considered that the targets of the inversion were the blocks with positive density contrasts. Thus, we used the ℓ_1 norm of the residuals to “ignore” the gravitational effect of the other non-targeted sources and recover only the blocks with positive density contrasts.

The synthetic data set contains 625 values of the g_{yy} , g_{yz} , and g_{zz} components, totaling 1,875 values. We corrupted the data with a pseudorandom Gaussian error of standard deviation 0.5 Eötvös and zero mean to simulate measurement errors. The interpretative model consists of 37,500 juxtaposed rectangular prisms. Our starting configuration is composed of one seed for the block with density contrast 0.6 g.cm^{-3} (yellow prism in Figure 3c) and 13 seeds for the two blocks with density contrast 1.0 g.cm^{-3} (red prisms in Figure 3c).

Figure 2a-c shows the adjustment of the data produced by estimated density-contrast distribution (Figure 3b) to the synthetic data. For comparison, the gravitational effects of the blocks with negative density contrast were removed from the synthetic data and plotted against the data produced by the estimate (Figure 2d-f). Notice that the inversion performed on the full synthetic data was able to fit the gravitational effects of the blocks with positive density contrasts. This demonstrates that our method is able to “ignore” the gravitational effect of the blocks with negative density contrast by allowing large residuals in places where this effect is dominant. Figure 3b shows that the estimated density-contrast distribution recovers only the three blocks with positive density contrasts.

APPLICATION TO REAL DATA

We applied our algorithm to a Full Tensor Gradiometry (FTG) survey over iron ore deposit of the Cauê Itabirite located in the region known as Quadrilátero Ferrífero, Brazil. We chose to use the g_{yy} , g_{yz} , and g_{zz} components in the inversion because

Robust 3D gravity gradient inversion

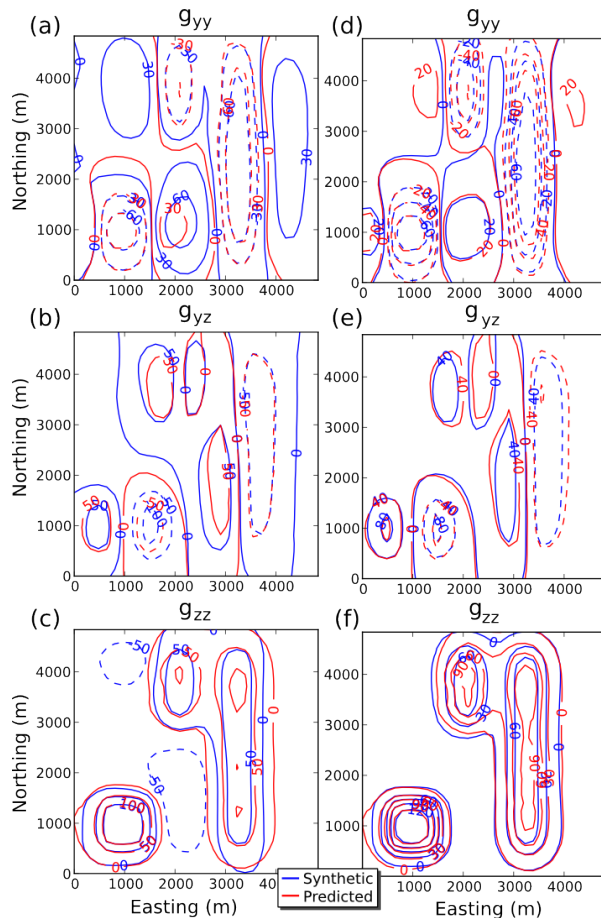


Figure 2: Test with synthetic data. **a-c)** Synthetic noise-corrupted data and data predicted by the inversion for the three components used. **d-f)** For comparison, the effect of the prisms with negative density contrast was removed from the synthetic data and the result is shown in blue contours. The data predicted by the inversion remains the same as in a-c.

the elongated SW-NE feature related to the iron ore deposits is more prominent in these components (Figure 4a-c). The data were terrain corrected using a density of 2.67 g.cm^{-3} . Assuming an iron ore deposit with density of 3.67 g.cm^{-3} results in a density contrast of 1.0 g.cm^{-3} between the ore and host rocks. This value was assigned to all seeds in the inversion. The data set contains 4582 measurements of each component, resulting in a total of 13,746 measurements. The interpretative model consists of 164,892 prisms that included the topography of the area. We used 46 seeds whose locations were chosen based on the g_{zz} component map and previous geologic models of the area.

Figure 5 shows the estimated 3D density-contrast distribution which is composed of compact geologic bodies that are in close agreement with previous interpretations by Martinez et al. (2010). Figure 4d-f shows the data predicted by the inversion. Notice that, for all three components, the inversion is able to fit the elongated SW-NE feature and consider as outliers the gravitational effects of other sources. When performed on a computer with an Intel® Core™ 2 Duo P7350 2.0 GHz pro-

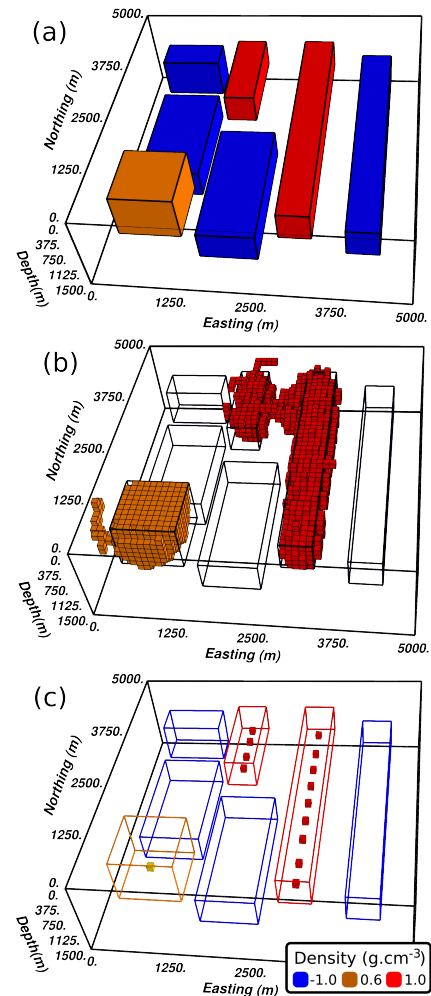


Figure 3: Test with synthetic data. **a)** Prismatic model used to generate the three component synthetic data. **b)** Inversion results using the ℓ_1 norm. All prisms with density contrast different from zero are shown. Contours of the synthetic model also shown for comparison. **c)** Set of seeds used in the inversion (yellow and red prisms).

cessor, the total time for the inversion was approximately 15 minutes.

CONCLUSIONS

We have presented a new method for the 3D inversion of gravity gradient data that uses a systematic search algorithm and a robust adjustment through the use of the ℓ_1 norm of the residuals. Prior information is incorporated into the solution by means of prismatic elements called “seeds” around which the solution is concentrated. Large data sets and fine interpretative models can be easily handled by implementing a “lazy evaluation” of the Jacobian matrix. Synthetic and field data tests show that our method is able to recover compact bodies with different density contrasts despite the presence of interfering gravitational effects produced by non-targeted sources. Thus, prior knowledge of density-contrast values and seed locations for these sources is not required.

Robust 3D gravity gradient inversion

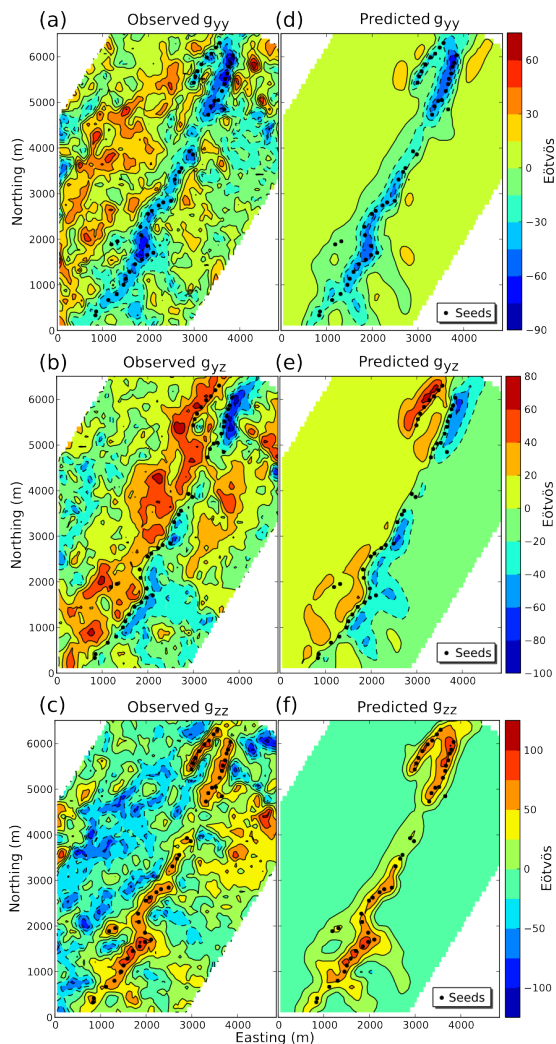


Figure 4: FTG data from Quadrilátero Ferrífero. **a-c)** Observed g_{yy} , g_{yz} , and g_{zz} components. **d-f)** g_{yy} , g_{yz} , and g_{zz} components predicted by the inversion. Seeds shown in black dots.

ACKNOWLEDGMENTS

This research is supported by the Brazilian agencies CNPq and CAPES. We thank Vale for permission to use the FTG data of the Quadrilátero Ferrífero.

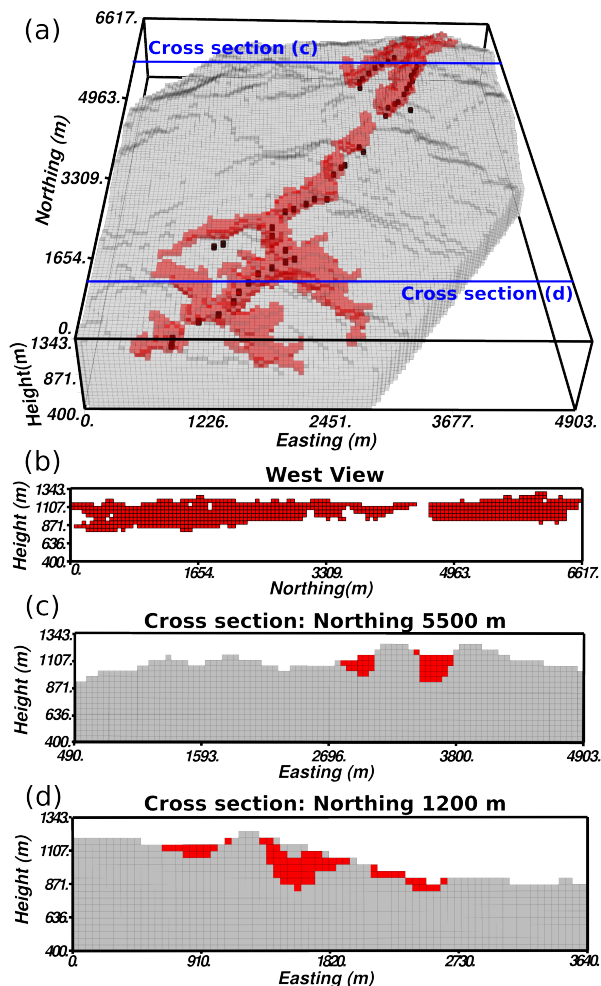


Figure 5: Result of the inversion of the FTG data from Quadrilátero Ferrífero. The “height” axis refers to height above the geoid. **a)** Prisms with zero density contrast shown in gray and prisms with density contrast 1.0 g.cm^{-3} shown in light red. Dark red prisms represent the seeds used in the inversion. Blue lines show the locations of cross sections (c) and (d). **b)** View of the result from the western side. **c)** Cross section at northing coordinate 5500 m. **d)** Cross section at northing coordinate 1200 m.

EDITED REFERENCES

Note: This reference list is a copy-edited version of the reference list submitted by the author. Reference lists for the 2011 SEG Technical Program Expanded Abstracts have been copy edited so that references provided with the online metadata for each paper will achieve a high degree of linking to cited sources that appear on the Web.

REFERENCES

- Camacho, A. G., F. G. Montesinos, and R. Vieira, 2000, Gravity inversion by means of growing bodies: *Geophysics*, **65**, 95–101, [doi:10.1190/1.1444729](https://doi.org/10.1190/1.1444729).
- Li, Y., and D. W. Oldenburg, 1998, 3-D inversion of gravity data: *Geophysics*, **63**, 109–119, [doi:10.1190/1.1444302](https://doi.org/10.1190/1.1444302).
- Martínez, C., Y. Li, R. Krahenbuhl, and M. Braga, 2010, 3D Inversion of airborne gravity gradiometry for iron ore exploration in Brazil: 80th Annual International Meeting, SEG, Expanded Abstracts, 1753–1757.
- Nagy, D., G. Papp, and J. Benedek, 2000, The gravitational potential and its derivatives for the prism: *Journal of Geodesy*, **74**, 552–560, [doi:10.1007/s001900000116](https://doi.org/10.1007/s001900000116).
- Portniaguine, O., and M. S. Zhdanov, 2002, 3-D magnetic inversion with data compression and image focusing: *Geophysics*, **67**, 1532–1541, [doi:10.1190/1.1512749](https://doi.org/10.1190/1.1512749).
- René, R. M., 1986, Gravity inversion using open, reject, and “shape-of-anomaly” fill criteria: *Geophysics*, **51**, 988–994, [doi:10.1190/1.1442157](https://doi.org/10.1190/1.1442157).
- Silva Dias, F. J. S., V. C. F. Barbosa, and J. B. C. Silva, 2009, 3D gravity inversion through an adaptive-learning procedure: *Geophysics*, **74**, no. 3, I9–I21, [doi:10.1190/1.3092775](https://doi.org/10.1190/1.3092775).